Acta Crystallographica Section B
Structural Science
ISSN 0108-7681

Structure, phase transitions and ionic conductivity of $K_3NdSi_6O_{15}\cdot xH_2O$. I. α-$K_3NdSi_6O_{15}\cdot 2H_2O$ and its polymorphs

S. M. Haile[a]* and B. J. Wuensch[b]

[a]Materials Science, California Institute of Technology, Pasadena, CA 91125, USA, and [b]Department of Materials Science and Engineering, Massachusetts Institute of Technology, Cambridge, MA 02139-4307, USA

Correspondence e-mail: smhaile@caltech.edu

Received 26 April 1999
Accepted 6 December 1999

Hydrothermally grown crystals of α-$K_3NdSi_6O_{15}\cdot 2H_2O$, potassium neodymium silicate, have been studied by single-crystal X-ray methods. The compound crystallizes in space group *Pbam*, contains four formula units per unit cell and has lattice constants a = 16.008 (2), b = 15.004 (2) and c = 7.2794 (7) Å, giving a calculated density of 2.683 Mg m^{-3}. Refinement was carried out with 2161 independent structure factors to a residual, $R(F)$, of 0.0528 [$wR(F^2)$ = 0.1562] using anisotropic temperature factors for all atoms other than those associated with water molecules. The structure is based on highly corrugated $(Si_2O_5^{2-})_\infty$ layers which can be generated by the condensation of xonotlite-like ribbons, which can, in turn, be generated by the condensation of wollastonite-like chains. The silicate layers are connected by Nd octahedra to form a three-dimensional framework. Potassium ions and water molecules are located in interstitial sites within this framework, in particular, within channels that extend along [001]. Aging of as-grown crystals at room temperature for periods of six months or more results in an ordering phenomenon that causes the length of the c axis to double. In addition, two phase transitions were found to occur upon heating. The high-temperature transformations, investigated by differential scanning calorimetry, thermal gravimetric analysis and high-temperature X-ray diffraction, are reversible, suggesting displacive transformations in which the layers remain intact. Conductivity measurements along all three crystallographic axes showed the conductivity to be greatest along [001] and further suggest that the channels present in the room-temperature structure are preserved at high temperatures so as to serve as pathways for easy ion transport. Ion-exchange experiments revealed that silver can readily be incorporated into the structure.

1. Introduction

In a contribution to silicate crystal chemistry, Pushcharovskii *et al.* (1977) reported the structure of a new rare-earth silicate, $K_3NdSi_6O_{15}$. No physical properties of the material were examined. However, connected channels between corrugated $(Si_2O_5^{2-})_\infty$ layers in the structure contained alkali ions, whose large isotropic temperature factors suggested residence in shallow potential minima. These characteristics attracted our attention to the phase as a possible fast-ion conductor. The possibilities of substituting other rare-earth ions of different radius or valence for Nd^{3+} (thus changing the dimensions of the framework, the concentration of charge-carrying alkali ions and/or the number of vacancies in the alkali-ion sites) or replacing K^+ by smaller alkali ions better matched to pathways in the structure, all suggested a flexible system amenable to crystal-chemical tailoring to optimize conduction. The mate-

rial, at the very least, promised opportunity for interesting structure–property correlations.

The conditions under which crystals of $K_3NdSi_6O_{15}$ had been originally produced were not reported. We therefore explored the hydrothermal conditions under which crystals of the phase could be successfully grown (Haile, Siegrist *et al.*, 1991; Haile *et al.*, 1993). A preliminary determination of the structure of the crystals we obtained was performed to insure that the phase was the same as that examined by Pushcharovskii *et al.* (1977). The introduction of anisotropic temperature factors for the K and Nd atoms, and further refinement reduced the residual, $R(F)$, to 0.083 from the value of 0.093 obtained by Pushcharovskii and coworkers, thereby confirming our crystals to be of the same phase as those previously examined (Haile, Siegrist *et al.*, 1991).

The present paper presents the results of extensive examination of the structure and thermal behavior of α-$K_3NdSi_6O_{15}\cdot 2H_2O$. A reanalysis of the room-temperature structure with new single-crystal X-ray diffraction data in combination with the thermal analyses leads to the conclusion that the original phase, to be designated α, is actually a hydrate. Furthermore, we present evidence for two reversible transformations, at elevated temperatures, to phases designated α_I and α_{II}, as well as describing a curious aging phenomenon of crystals of the α phase. After synthesis, prolonged 'annealing' under ambient conditions resulted in the formation of a superstructure, α', in which the length of the c axis was doubled (Haile, Wuensch *et al.*, 1991). Moreover, the ionic conductivity of α_{II} is reported, along with the results of preliminary attempts to effect ion exchange of Ag^+ for K^+ as a means of enhancing conductivity.

In addition to α, a second, essentially isocompositional phase was occasionally obtained from hydrothermal syntheses that were performed in the high-silica end of the K_2O–Nd_2O_3–SiO_2 system. This phase, to be designated β, appears to be anhydrous and was found to contain a silicate sheet of the same connectivity, but with a distinct polymorphic conformation relative to that in the structure of α. A description of the structure of β is reported separately in a companion paper (Haile & Wuensch, 2000).

2. Experimental

2.1. Synthesis and phase identification

Crystals of α-$K_3NdSi_6O_{15}\cdot 2H_2O$ were grown hydrothermally using both isothermal and temperature–gradient techniques, as described elsewhere (Haile *et al.*, 1993). Hydrothermal techniques employ high temperatures and pressures to dissolve a normally insoluble precursor material and precipitate the stable crystalline phase (Laudize, 1987) and are particularly suited to inducing crystallization in silicates that otherwise form glasses when cooled from the melt. The range of conditions that yielded the present compound are summarized in Table 1. In the vast majority of both the isothermal and temperature–gradient experiments carried out, crystals of α-$K_3NdSi_6O_{15}\cdot 2H_2O$ grew as fragile (100) orthorhombic plates. Striations were apparent along both [010] and [001]. Prior to electrical, thermal or compositional characterization, the phase of each crystal was confirmed by single-crystal diffraction methods, primarily precession photography (Mo $K\alpha$ radiation). On occasion, the time between synthesis and further experimentation was as long as several months, and single-crystal diffraction analysis of aged samples showed additional diffraction peaks compared with freshly synthesized samples. These were, again, recorded by precession photography.

Table 1
The hydrothermal conditions under which α-$K_3NdSi_6O_{15}\cdot 2H_2O$ was synthesized.

Experiment	Isothermal range	Isothermal optimum	Gradient
Autoclave	Tuttle	Tuttle	Morey
Pressure control	External	External	Implicit
Reaction volume (cm^3)	0.20–0.25	0.20	30
Nutrient	47–62 mg glass† or 29 mg SiO_2 + 9.5–14 mg Nd_2O_3 + 0–50 mg K_2CO_3	50 mg glass	1.26 g Nd_2O_3, 2.69 g SiO_2‡
Low temperature (K)	57–873	773	608
High temperature (K)	(As above)	(As above)	698
Pressure (MPa)	82.5, 140	82.5	60§
Solvent/mineralizer	0–2*M* KOH 0–1*M* K_2CO_3 0.1*M* $K_2B_4O_7$	1*M* KOH	2*M* KOH
Fill (%)	30–70	48	63
Duration (d)	5–20	10	9
Crystal size (mm^3)	Microcrystalline	Microcrystalline	0.1 × 2 × 1

† Glass of composition $4K_2O$–Nd_2O_3–$17SiO_2$. ‡ Amorphous. § Estimated from pressure–volume–temperature data for pure water.

2.2. Determination of composition

The composition of α-$K_3NdSi_6O_{15}\cdot 2H_2O$ was determined through electron microprobe analysis. Crystals were mounted in an epoxy resin, polished and sputter-coated using a gold/palladium electrode. Data were collected with a Jeol Superprobe 733 equipped with a wavelength-dispersive detector. Measured intensities of the characteristic X-radiation peaks were converted to stoichiometric quantities using the *ZAF* data reduction program (Schamber *et al.*, 1981). The materials employed as standards were SiO_2 glass, a single crystal of NdF_3 and an orthoclase glass for K. The measurements yielded absolute mole percentages of K, Nd and Si of 9.55 (35), 3.51 (7) and 22.2 (5), respectively. These values are rather close to the ideal percentages of 9.68, 3.23 and 19.4, respectively, for $K_3NdSi_6O_{15}\cdot 2H_2O$. Conversion of the mole percentages of metals to weight percentages of the respective oxides provides a sum of 93.3 (12) wt%. Pushcharovskii and coworkers' study, as well as our earlier reanalysis of the phase, assumed it to be anhydrous. However, if the balance of 6.7 wt% is taken to be due to water, the deficiency is close to a value of 5.1 wt% that would be expected for ideal $K_3NdSi_6O_{15}\cdot 2H_2O$.

Table 2
Experimental details.

Crystal data	
Chemical formula	$H_4K_3NdSi_6O_{17}$
Chemical formula weight	706.1
Cell setting	Orthorhombic
Space group	*Pbam*
a (Å)	16.008 (2)
b (Å)	15.004 (2)
c (Å)	7.2794 (7)
V (Å^3)	1748.4 (3)
Z	4
D_x (Mg m^{-3})	2.683
Radiation type	Mo $K\alpha$
Wavelength (Å)	0.71073
No. of reflections for cell parameters	20
μ (mm^{-1})	4.178
Temperature (K)	293 (2)
Crystal size (mm)	0.5 × 0.4 × 0.2
Data collection	
Diffractometer	Siemens *R*3*m*–V
Absorption correction	ψ scan (empirical)
T_{min}	0.061
T_{max}	0.102
No. of measured reflections	2579
No. of independent reflections	2173
No. of observed reflections	1897
Criterion for observed reflections	$I \geq 2\sigma$
R_{int}	0.0204
θ_{max} (°)	27.51
Range of h, k, l	$0 \rightarrow h \rightarrow 20$ $0 \rightarrow k \rightarrow 19$ $-9 \rightarrow l \rightarrow 9$
Refinement	
Refinement on	F^2
$R[F^2>2\sigma(F^2)]$	0.0528
$wR(F^2)$	0.1562
S	1.016
No. of reflections used in refinement	2161
No. of restraints/parameters	1/144
H-atom treatment	H atoms not located
Weighting scheme	$w = 1/[\sigma^2F_o^2 + (0.0816P)^2 + 30.48P]$, where $P = [\max(F_o^2,0) + 2F_c^2]/3$
$\Delta\rho_{max}$ (e Å^{-3})	2.494
$\Delta\rho_{min}$ (e Å^{-3})	−1.765
Extinction method	None
Source of atomic scattering factors	Cromer & Waber (1974)
Computer programs	
Structure refinement	*SHELXL* (Sheldrick, 1993)

2.3. Thermal analysis

Thermogravimetric analysis was performed to obtain a quantitative measure of water content. Weight loss, while heating at a rate of 10–20 K min^{-1} and under low vacuum conditions ($\sim 10^{-3}$ Pa), was recorded with a Netzsch thermogravimetric balance (model STA). As shown below, gradual weight loss occurred over the temperature range 325–525 K and mass spectrometry of the evolved gas confirmed it to be comprised entirely of water vapor. The total weight change was 3.0 wt% which, with the results of microprobe analysis, brackets the value of 5.1 wt% to be expected for ideal $K_3NdSi_6O_{15}\cdot 2H_2O$. The phase, accordingly, is not anhydrous as originally assumed, a conclusion that is confirmed by the present structure analysis.

Because of the relatively high temperatures required to obtain measurable conductivities, samples were examined for possible phase transformations using differential scanning calorimetry (DSC) and high-temperature X-ray powder diffraction. Thermal analysis was performed in flowing N_2 on powdered samples with a Perkin Elmer DSC7 over the temperature range 323–873 K and with a Seiko DSC-320 for higher temperatures (up to 1373 K). The heating rate was 10–20 K min^{-1}, and samples 5–30 mg in mass. The high-temperature diffractometry is described below.

2.4. Collection and refinement of room-temperature diffraction data

Crystal data and details of the collection of single-crystal diffraction data are provided in Table 2.[1] Systematic absences showed the diffraction symbol to be *mmm Pba**. The lattice constants and diffraction symbol agree with those of Pushcharovskii *et al.* (1977) and our earlier study (Haile, Siegrist *et al.*, 1991) reported for the same phase. The space group was taken to be *Pbam* and, in accordance with the earlier results, an anhydrous model initially assumed.

Refinement of this model, consisting of 19 non-water atoms, proceeded only to a residual, $wR(F^2)$, of ∼0.21 with $R(F) \simeq 0.075$. A difference map revealed significant residual electron density at three sites, the first with a maximum density of 7 e Å^{-3} and two containing 3 e Å^{-3}. Partial occupancy of O atoms belonging to water molecules, O*w*, was therefore assigned to these locations. Doing so lowered the residuals significantly and provided additional coordination to potassium ions, as discussed below. The three occupancy factors were fixed so as to sum to a total of two H_2O molecules per formula unit (to conform to the results of the TGA and microprobe analyses). As the interstitial site occupancies strongly correlate with the temperature factors of these atoms, the three occupancy factors were adjusted to yield refined values of the isotropic temperature-factor coefficients for the three O*w* species which were approximately equal. This was found to occur for occupancies close to 2/3, 1/3 and 1/3 (which, it may be noted, are in approximately the same ratio as the corresponding residual densities in the difference map). The O*w* site occupancies were, accordingly, fixed at these rational fractions in the final cycles of refinement. Anisotropic temperature factors were employed for all other atoms. Using all but the very negative data [2161 reflections with $I \geq -2\sigma(I)$], a final residual, $wR(F^2)$, of 0.1562 was obtained. Structure-factor calculations and least-squares refinement for the structure were carried out using the *SHELXL*93 program (Sheldrick, 1993), in which a residual based on F^2 was minimized. Further details of the refinement are given in Table 2.

[1] Supplementary data for this paper are available from the IUCr electronic archives (Reference: BS0005). Services for accessing these data are described at the back of the journal.

Table 3
Atomic coordinates determined for α-$K_3NdSi_6O_{15}\cdot 2H_2O$.

The compound crystallizes in space group *Pbam*, and has lattice constants a = 16.008 (2), b = 15.004 (2) and c = 7.2794 (7) Å. O*w* indicates the location of an oxygen atom associated with a water molecule. The coordinates in italics listed below the results of the present work are the values originally reported by Pushcharovskii *et al.* (1977) and are provided for comparison.

	Position	*x*	*y*	*z*
Nd(1)	2(*a*) ..2/*m*	0	0	0
Nd(2)	2(*c*) ..2/*m*	1/2	0	0
K(1)	4(*g*) ..*m*	0.2910 (3)	0.3785 (3)	0
		0.2912	*0.3791*	
K(2)	4(*h*) ..*m*	0.1556 (2)	0.1555(3)	1/2
		0.1548	*0.1561*	
K(3)	4(*h*) ..*m*	0.0699 (2)	0.4105 (2)	1/2
		0.0705	*0.4115*	
Si(1)	4(*g*) ..*m*	0.21036 (14)	0.1268 (2)	0
		0.2101	*0.1274*	
Si(2)	8(*i*) 1	0.35548 (10)	0.13505 (11)	0.2862 (2)
		0.3551	*0.1352*	*0.2865*
Si(3)	4(*g*) ..*m*	0.0912 (2)	0.2806 (2)	0
		0.0909	*0.2802*	
Si(4)	8(*i*) 1	0.46288 (11)	0.29877 (11)	0.2821 (3)
		0.4624	*0.2992*	*0.2826*
O(1)	8(*i*) 1	0.0429 (4)	0.2459 (3)	0.1828 (8)
		0.043	*0.244*	*0.182*
O(2)	4(*g*) ..*m*	0.1018 (5)	0.3859 (5)	0
		0.102	*0.383*	
O(3)	4(*g*) ..*m*	0.1822 (4)	0.2318 (4)	0
		0.183	*0.231*	
O(4)	4(*g*) ..*m*	0.1346 (4)	0.0599 (4)	0
		0.135	*0.061*	
O(5)	8(*i*) 1	0.2689 (3)	0.1134 (3)	0.1799 (7)
		0.263	*0.144*	*0.180*
O(6)	4(*h*) ..*m*	0.3264 (4)	0.1335 (5)	1/2
		0.323	*0.133*	
O(7)	8(*i*) 1	0.4289 (3)	0.0679 (3)	0.2459 (8)
		0.427	*0.070*	*0.246*
O(8)	8(*i*) 1	0.3803 (3)	0.2390 (3)	0.2397 (8)
		0.379	*0.239*	*0.239*
O(9)	8(*i*) 1	0.4477 (3)	0.3984 (3)	0.2213 (8)
		0.448	*0.397*	*0.222*
O(10)	4(*h*) ..*m*	0.4846 (5)	0.2876 (5)	1/2
		0.486	*0.287*	
O*w*(1)†	4(*h*) ..*m*	0.3659 (10)	0.4830 (10)	1/2
O*w*(2)‡	8(*i*) 1	0.2281 (13)	0.3284 (14)	0.421 (3)
O*w*(3)‡	8(*i*) 1	0.2113 (13)	0.4189 (14)	0.292 (3)

† Occupancy fixed at 2/3, atom not reported by Pushcharovskii *et al.* (1977). ‡ Occupancy fixed at 1/3, atom not reported by Pushcharovskii *et al.* (1977).

2.5. High-temperature X-ray diffraction

The thermal analysis revealed that α-$K_3NdSi_6O_{15}\cdot 2H_2O$ undergoes structural phase transitions at slightly elevated temperatures and prompted high-temperature X-ray diffraction investigations. Three techniques were pursued for obtaining high-temperature data. Photographic data from powder samples were collected using a Guinier camera equipped with a furnace and a moving cassette (Simon, 1971). Samples were placed in a closed capillary and heated at a rate of $\sim$20 K h^{-1} to 673 K and then brought back to room temperature. Diffractometer data were obtained, again, from powder samples, utilizing a Philips PW1820 goniometer equipped with an Anton Parr HTK-10 furnace. Diffraction experiments were carried out at room temperature, 393 and 493 K, on both heating and cooling. Cu $K\alpha$ radiation was used for both sets of powder experiments. Single crystal data from heated samples were recorded on film by precession photography (Mo $K\alpha$ radiation). Samples were heated using a custom-built furnace, which gave a temperature control of $\pm$15 K.

2.6. Conductivity and ion exchange

The hydrothermal syntheses yielded crystals large enough (up to 2 mm on edge) and in great enough quantity to permit the measurement of the complete conductivity tensor, σ_{ij}. Electrodes were attached to either end of the single-crystal samples for which the relationship between crystal morphology and internal axes had been determined from X-ray photographic techniques. Either a platinum paste, cured at 1173 K, or a silver epoxy, cured at 473 K, served as the

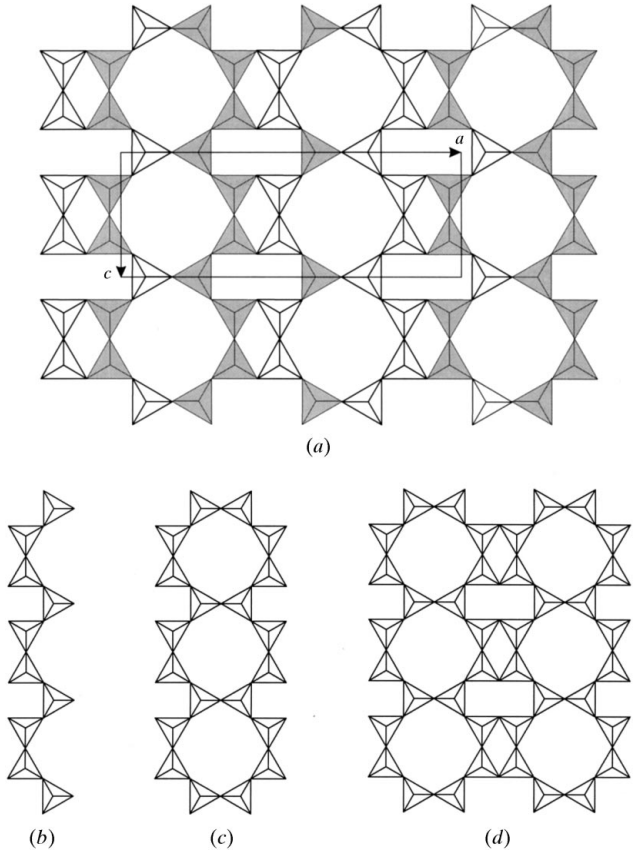

Figure 1
(*a*) Idealized representation of the linkage of silica tetrahedra in the (Si_2O_5) layer parallel to (010) in α-$K_3NdSi_6O_{15}\cdot 2H_2O$. In the actual structure the layer is highly corrugated (with corrugations running along *c*), whereas in this representation all tetrahedra are oriented such that the face composed of three bridging oxygen atoms is exactly parallel to (010). Tetrahedra for which the terminating vertex is below the plane formed by the three bridging vertices (downward directed) are shaded. Those oriented in the opposite direction are not. (*b*) The wollastonite chain with a three-tetrahedra periodicity. (*c*) Condensation of two wollastonite chains to form the xonotlite double chain having a sequence of eight-membered rings. (*d*) Coalescence of a pair of xonotlite chains to form a portion of the Si_2O_5 layer found in α-$K_3NdSi_6O_{15}\cdot 2H_2O$. Four- and six-membered rings alternate along the interface between the xonotlite ribbons.

Table 4
Refined anisotropic temperature-factor coefficients for α-$K_3NdSi_6O_{15}\cdot 2H_2O$.

Anisotropic temperature factors are of the form $\exp[-2\pi^2(h^2U^{11}a^{*2} + ... + hkU^{12}a^*b^* + ...)]$ and are given in units of 10^{-2} Å^2. U_{iso} is $1/3(U^{11} + U^{22} + U^{33})$.

Atom	U_{iso}	U^{11}	U^{22}	U^{33}	U^{23}	U^{13}	U^{12}
Nd(1)	1.50 (2)	1.39 (4)	1.31 (3)	1.79 (4)	0	0	−0.02 (2)
Nd(2)	1.73 (2)	1.79 (4)	1.43 (4)	1.96 (4)	0	0	0.11 (2)
K(1)	7.88 (13)	6.3 (2)	6.9 (2)	10.5 (4)	0	0	−4.0 (2)
K(2)	6.08 (9)	3.8 (2)	7.3 (2)	7.1 (2)	0	0	0.8 (2)
K(3)	5.83 (10)	3.34 (14)	4.5 (2)	9.6 (3)	0	0	−0.12 (12)
Si(1)	1.41 (5)	1.24 (11)	1.41 (10)	1.56 (11)	0	0	−0.16 (8)
Si(2)	1.62 (4)	1.71 (8)	1.70 (8)	1.44 (8)	−0.06 (6)	−0.03 (6)	0.03 (6)
Si(3)	1.75 (5)	1.57 (11)	1.69 (11)	2.00 (12)	0	0	0.23 (9)
Si(4)	1.80 (4)	2.16 (8)	1.70 (8)	1.53 (8)	0.12 (7)	0.17 (7)	−0.23 (6)
O(1)	3.11 (12)	2.7 (3)	3.9 (3)	2.8 (3)	0.1 (2)	0.7 (2)	−0.3 (2)
O(2)	3.0 (2)	2.1 (3)	1.7 (3)	5.0 (5)	0	0	0.7 (3)
O(3)	2.28 (14)	1.7 (3)	1.6 (3)	3.4 (4)	0	0	0.1 (3)
O(4)	2.23 (14)	1.6 (3)	1.8 (3)	3.2 (4)	0	0	−0.3 (2)
O(5)	2.65 (11)	2.9 (2)	2.7 (2)	2.3 (2)	0.5 (2)	−1.0 (2)	−0.9 (2)
O(6)	2.41 (14)	1.9 (3)	3.5 (4)	1.8 (3)	0	0	0.0 (3)
O(7)	2.70 (11)	2.3 (2)	2.5 (2)	3.3 (3)	−0.4 (2)	0.5 (2)	0.4 (2)
O(8)	2.37 (11)	2.6 (2)	1.8 (2)	2.7 (3)	0.2 (2)	−0.2 (2)	−0.2 (2)
O(9)	2.80 (11)	3.6 (3)	1.9 (2)	2.9 (3)	0.6 (2)	0.2 (2)	−0.2 (2)
O(10)	2.6 (2)	3.4 (4)	2.4 (4)	1.9 (3)	0	0	−0.0 (3)
O*w*(1)	4.9 (4)						
O*w*(2)	5.2 (5)						
O*w*(3)	5.1 (5)						

electrode material. Impedance data were collected, at high temperatures (> 873 K), with an HP4102A inductance–capacitance–resistance (LCR) meter over the frequency range 5 Hz to 13 MHz and with an applied voltage of 500 mV. Lower-temperature measurements were performed with a single frequency ($\omega = 10^4$ Hz) Wayne-Kerr B642 autobalance bridge. Data were collected in air at 25 to 50 K intervals over the temperature range 573–1173 K. Samples were allowed to equilibrate for approximately 30 min at each temperature prior to the measurement of the conductivity.

Ion exchange experiments were performed by soaking crystals in a 1*M* solution of $AgNO_3$ for 2 weeks. Samples were protected from light during this period to prevent photo-induced oxidation or reduction of Ag^+. Both before and after ion exchange, crystals were examined by X-ray precession photography. These crystals were unfortunately too small for conductivity measurements, and of too poor crystalline quality, as a result of the exchange, for full structure determination and/or refinement. Nevertheless, distinct differences between the two sets of precession photographs were readily observable.

3. Room-temperature structure

3.1. Results

The atomic coordinates and thermal parameters of the atoms in α-$K_3NdSi_6O_{15}\cdot 2H_2O$ are reported in Tables 3 and 4, respectively. Bond lengths for the silicon and neodymium coordination polyhedra in α-$K_3NdSi_6O_{15}\cdot 2H_2O$ are given in Table 5. Oxygen to oxygen distances and bond angles are also provided for the silica tetrahedra. O atoms that form bonds to two Si atoms are designated 'bridging' (O_{br}) to denote their role in the silica framework, whereas those that bond to only one are designated 'terminating' (O_t). The distances between potassium ions and their anion neighbors are presented in Table 6, whereas distances between interstitial water molecules and their nearest neighbors are listed in Table 7. For the present purposes, nearest anion neighbors to potassium ions are defined as those which are closer to the potassium than its nearest cation neighbor, which turns out to be a distance of ~ 3.5 Å. Anion next-nearest neighbors are defined as those at distances of $\sim$ 3.5 to 4.0 Å from potassium. In addition to these distances, the sum of the bond valences at the potassium ions are also given in Table 6 and these data are discussed further below. The bond-valence sum, $\sum S$, has been calculated assuming a single K—O bond valence of $\exp[(2.132 - d_{K-O}\,\text{Å})/0.37]$ (Brown & Altermatt, 1985). The present results (coordinates, bond distances, *etc.*) have somewhat improved standard deviations over those previously reported (Haile, Siegrist *et al.*, 1991).

3.2. Discussion

3.2.1. Silica–neodymia framework. The structure of α-$K_3NdSi_6O_{15}\cdot 2H_2O$ is based on 'ideal' $(Si_2O_5^{2-})_\infty$ layers, that is, layers in which all SiO_4 tetrahedra have three bridging O atoms (linked to other tetrahedra) and one terminating oxygen vertex. The tetrahedra themselves exhibit rather typical bond lengths (Liebau, 1987): the average Si—O_t and Si—O_{br} distances are 1.579 (6) and 1.628 (8) Å, respectively, Table 5. The difference between the two averages of ~ 0.04 Å is also quite typical for silicate structures and reflects the stronger bonding between Si and O_t compared with that between Nd and O (or between K and O). In addition, the average O—O distances and the average O—Si—O bond angles, 2.64 (4) Å and 109 (4)°, respectively, are also very similar to values reported in the literature.

The Si_2O_5 layers in α-$K_3NdSi_6O_{15}\cdot 2H_2O$ extend along (010). An idealized planar representation of the linkage in one such layer (at $y \simeq \frac{1}{4}$ in the structure) is shown in Fig. 1*a*, in which all tetrahedra have been oriented such that the face composed of bridging O atoms is parallel to (010). Tetrahedra which are directed 'downwards', *i.e.* have their terminal vertex below the plane formed by the three bridging O atoms, are shaded, whereas those which are directed 'upwards' (along **b**) are unshaded. The sheet contains four-, six- and eight-membered rings. Liebau (1962) proposed that silicate layers be classified on the basis of the nature of a silicate chain from which the

Table 5
Interatomic distances (Å) and bond angles (°) in the neodymium and silicon coordination polyhedra in β-$K_3NdSi_6O_{15}\cdot 2H_2O$.

	Bond distance (Å)		Oxygen separation along edge (Å)		O—*M*—O angle (°)
Nd(1)	O(4), O(4)^{i}	2.334 (6)	O(4)—O(9) 4×	3.193 (7)	85.5 (2)
	O(9)^{ii}, O(9)^{iii}	2.371 (5)	O(4)—O(9) 4×	3.455 (8)	94.5 (2)
	O(9)^{iv}, O(9)^{v}	[2.371 (5)]	O(9)—O(9) 2×	3.221 (11)	85.6 (3)
			O(9)—O(9) 2×	3.479 (10)	94.4 (3)
	Average	2.36(2)		3.33 (14)	
Nd(2)	O(7)^{vi}, O(7)^{vii}	2.354 (5)	O(7)—O(7) 2×	3.056 (9)	81.0 (3)
	O(7), O(7)^{viii}	[2.354 (5)]	O(7)—O(7) 2×	3.581 (11)	99.0 (3)
	O(2)^{ii}, O(2)^{ix}	2.364 (7)	O(7)—O(2) 4×	3.303 (8)	88.9 (2)
			O(7)—O(2) 4×	3.369 (8)	91.1 (2)
	Average	2.359 (7)		3.33 (16)	
Si(1)	$O(4)_t$	1.575 (7)	O(4)—O(5) 2×	2.642 (7)	111.5 (2) 2×
	$O(5)_{br}$	1.623 (5)	O(4)—O(3)	2.690 (9)	113.7 (4)
	$O(5)_{br}{}^{viii}$	1.623 (5)	O(5)—O(5)	2.619 (11)	107.6 (4)
	$O(3)_{br}$	1.639 (7)	O(5)—O(3) 2×	2.607 (8)	106.1 (2) 2×
Si(2)	$O(7)_t$	1.575 (5)	O(7)—O(5)	2.694 (7)	114.9 (3)
	$O(5)_{br}$	1.621 (5)	O(7)—O(6)	2.661 (7)	112.5 (3)
	$O(6)_{br}$	1.624 (3)	O(7)—O(8)	2.682 (7)	112.8 (3)
	$O(8)_{br}$	1.644 (5)	O(5)—O(6)	2.524 (6)	102.1 (3)
			O(5)—O(8)	2.631 (7)	107.4 (3)
			O(6)—O(8)	2.615 (7)	106.3 (3)
Si(3)	$O(2)_t$	1.588 (7)	O(2)—O(1) 2×	2.659 (8)	111.7 (2) 2×
	$O(1)_{br}{}^{viii}$	1.625 (6)	O(2)—O(3)	2.645 (10)	110.5 (4)
	$O(1)_{br}$	1.625 (6)	O(1)—O(1)	2.662 (12)	110.0 (4)
	$O(3)_{br}$	1.631 (7)	O(1)—O(3) 2×	2.605 (8)	106.3 (3) 2×
Si(4)	$O(9)_t$	1.578 (5)	O(9)—O(1)	2.663 (7)	113.0 (3)
	$O(1)_{br}{}^{ix}$	1.617 (6)	O(9)—O(8)	2.627 (7)	110.1 (3)
	$O(8)_{br}$	1.627 (5)	O(9)—O(10)	2.689 (7)	113.8 (4)
	$O(10)_{br}$	1.632 (3)	O(1)—O(8)	2.646 (8)	109.3 (3)
			O(1)—O(10)	2.541 (7)	102.9 (4)
			O(8)—O(10)	2.629 (7)	107.5 (4)

$\langle Si—O_{term}\rangle$ = 1.579 (6), $\langle Si—O_{br}\rangle$ = 1.628 (8), $\langle O—O\rangle$ = 2.64 (4) Å and $\langle O—Si—O\rangle$ = 109 (4)°. Symmetry codes: (i) $-x, -y, -z$; (ii) $-x+\frac{1}{2}, y-\frac{1}{2}, -z$; (iii) $x-\frac{1}{2}, -y+\frac{1}{2}, z$; (iv) $-x+\frac{1}{2}, y-\frac{1}{2}, z$; (v) $x-\frac{1}{2}, -y+\frac{1}{2}, -z$; (vi) $-x+1, -y, z$; (vii) $-x+1, -y, -z$; (viii) x, y, z; (ix) $x+\frac{1}{2}, -y+\frac{1}{2}, z$.

sheet may be constructed. The Si_2O_5 layer in α-$K_3NdSi_6O_{15}\cdot 2H_2O$ may be built by coalescence of chains with a periodicity of three tetrahedra (*dreierkette*), such as occurs in wollastonite, $CaSiO_3$ (Buerger & Prewitt, 1961), Fig. 1(*b*). Condensation of a pair of wollastonite chains results in a double ribbon with a sequence of eight-membered rings, Fig. 1(*c*). This silicate unit is realised in the structure of xonotlite, $Ca_6Si_6O_{17}(OH)_2$ (Kudoh & Takéuchi, 1979). Coalescence, in turn, of xonotlite ribbons creates a sheet with a sequence of alternating four- and six-membered rings at the interface between the double chains (Fig. 1*d*) yielding a Si_2O_5 layer with the connectivity found in α-$K_3NdSi_6O_{15}\cdot 2H_2O$.

The non-bridging oxygen ions in the idealized layer of Fig. 1(*a*) are arranged such that a wollastonite chain in which all non-bridging vertices point in the same direction alternates with a second chain in which two of the three non-bridging oxygen are oppositely directed from the third. In none of the rings in the sheet, four-, six- or eight-membered, do all tetrahedra have the same orientation.

A silicate layer with the linkage of Fig. 1 (albeit in a highly distorted form and with a different distribution of upwards and downwards-directed tetrahedra) was first discovered in dalyite, $K_2ZrSi_6O_{15}$, by Fleet (1965) and attracted great interest: it represented a new type of Si_2O_5 layer with a connectivity completely distinct from the only two types that were then known – the connected hexagonal rings common to the micas and clay minerals, and the relatively rare combination of eight- and four-membered rings first found in apophyllite, $KCa_4(Si_2O_5)_4F\cdot 8H_2O$ (Taylor & Náray-Szabó, 1931). We have recently (Haile & Wuensch, 1997) assembled structural results for a number of $A_xMSi_6O_{15}$ compounds (*A* is an alkali or alkaline earth ion, and *M* is Y, Zr or Ti) and shown that their silicate layers are related by structure-building operations analogous to that of Fig. 1.

The layers in the actual structure of α-$K_3NdSi_6O_{15}\cdot 2H_2O$ are strongly corrugated, with corrugations running along **c**, the direction of the wollastonite chain. This may be seen in Fig. 2, a projection of the structure along [001]. This corrugation causes the lattice constants *a* and *c* to be shorter and longer, respectively, than those that would occur in an ideal flat layer with all Si—O bond distances equal to 1.62 Å: *a*(ideal) = 18.06, *a*(obs) = 16.008 (2); *c*(ideal) = 6.39, *c*(obs) = 7.2794 (7) Å. Alternate layers are related by the operation of a twofold rotation axis parallel to [001], resulting in a two-layer stacking sequence along **b** which is visible in Fig. 2. The relationship between alternating layers can also be seen in Fig. 3, a projection along [010]. (For clarity, individual Nd atoms rather than Nd polyhedra are shown in this projection.) From the view of the structure along **c** which is provided in Fig. 2, it is apparent that the corrugations in neighboring layers are rather well aligned. Indeed, apart from the orientation of the non-bridging vertices along **c**, the layers almost appear to be related by translation. Stated in other terms, the separation of Si atoms along **b** is rather uniform. As a result, the structure contains large channels along [001] (one example of which is the eight-gon highlighted by bold lines in Fig. 2). Fig. 3, however, reveals that the relation between neighboring layers is not that of a pseudo-translation along **b**. Upon projection of a layer along **b** onto its neighbor, the various types of rings are seen to be offset from one another along the *a* axis by a distance equivalent to the width of one (SiO_4) tetrahedral unit. Consequently, there is no channel of any significance along [010]. This is in marked contrast to $Na_3NdSi_6O_{15}\cdot 2H_2O$, a related phyllosilicate with a one-layer stacking sequence in which the alignment of layers results in the presence of

Table 6
Distances in α-$K_3NdSi_6O_{15}\cdot 2H_2O$ between potassium ions and their nearest neighbors and between potassium ions and their next-nearest oxygen neighbors.

The sum of the bond valences, ΣS, at each potassium site, both with and without the contribution of the O atoms within water molecules, are also provided.

K(1) neighbor	Distance (Å)	K(2) neighbor	Distance (Å)	K(3) neighbor	Distance (Å)
O*w*(3), O*w*(3)^{i}	2.56 (2)	O*w*(1)^{ii}	2.61 (2)	O*w*(3), O*w*(3)^{iii}	2.73 (2)
O(3)	2.806 (8)	O(6)	2.755 (8)	O*w*(2), O*w*(2)^{iii}	2.87 (2)
O(4)^{iv}	2.971 (8)	O(10)^{v}	2.867 (8)	O(7)^{v},O(7)^{vi}	2.936 (6)
O(9), O(9)^{i}	2.995 (6)	O*w*(2), O*w*(2)^{iii}	2.90 (2)	O(7)^{vii}, O(7)^{viii}	3.001 (6)
O(2)	3.031 (8)	O(5), O(5)^{iii}	3.020 (6)	O(10)^{v}	3.270 (8)
O(8), O(8)^{i}	3.077 (6)	O(1), O(1)^{iii}	3.228 (6)	O(1), O(1)^{iii}	3.407 (6)
O*w*(2), O*w*(2)^{i}	3.31 (2)				

Next neighbor	Distance (Å)	Next neighbor	Distance (Å)	Next neighbor	Distance (Å)
O(5)^{iv}, O(5)^{viii}	3.880 (7)	O(3), O(3)^{ix}	3.839 (3)	O(2), O(2)^{ix}	3.694 (1)
		O(4), O(4)^{ix}	3.927 (3)	O(6)^{viii}	3.736 (8)
ΣS without H_2O	ΣS with H_2O	ΣS without H_2O	ΣS with H_2O	ΣS without H_2O	ΣS with H_2O
0.72	0.96	0.64	0.91	0.66	0.79

Symmetry codes: (i) $x, y, -z$; (ii) $-x+\frac{1}{2}, y-\frac{1}{2}, -z+1$; (iii) $x, y, -z+1$; (iv) $-x+\frac{1}{2}, y+\frac{1}{2}, -z$; (v) $x-\frac{1}{2}, -y+\frac{1}{2}, z$; (vi) $x-\frac{1}{2}, \frac{1}{2}-y, 1-z$; (vii) $-x+\frac{1}{2}, y+\frac{1}{2}, -z+1$; (viii) $-x+\frac{1}{2}, y+\frac{1}{2}, z$; (ix) $x, y, z+1$.

channels in a direction perpendicular to the layers (Haile *et al.*, 1997).

The two independent neodymium polyhedra are both rather regular octahedra that connect the silicate layers *via* corner-sharing with SiO_4 tetrahedra to form the three-dimensional network shown in Fig. 2. Accordingly (excluding weaker bonds formed with K atoms), all O atoms either form bonds between two Si atoms or between one Si atom and one Nd atom. Such a situation might be expected *a priori* for charge-balance reasons. Of the 12 edges of both neodymium octahedra, three link SiO_4 tetrahedra within a layer above the NdO_6 group, three link SiO_4 tetrahedra within a layer beneath the NdO_6 group and six connect adjacent layers to one another. The average Nd—O bond length is 2.36 Å for both polyhedra, a typical value close to the sum of the ionic radii (Shannon & Prewitt, 1969). The average O—O edge length of 3.33 Å also lies within the range normally observed for NdO_6 octahedra. Both Nd ions are located at sites of ..2/*m* symmetry and hence all transpolyhedral angles are 180°. The remaining O—Nd—O angles differ from 90° by no more than 10°.

Further examination of Fig. 2, a figure that shows the internal crystal structure, reveals the origins of the external crystal habit. As stated earlier, crystals were obtained as platelets with their major faces parallel to {100}. A likely cleavage plane parallel to this form is shown in Fig. 2 by a dotted line. The (100) face formed as a result of cleavage in this manner is terminated by the corners of complete SiO_4 tetrahedra and by incomplete potassium polyhedra. This would appear to be an energetically favorable surface as no Si—O or Nd—O bonds are broken, and, accordingly, all Si and Nd atoms have their bonding requirements satisfied. The formerly bridging oxygen ions [(between Si(4) and Si(3)] at the surface may well pick up a proton to fulfill their bonding requirements.

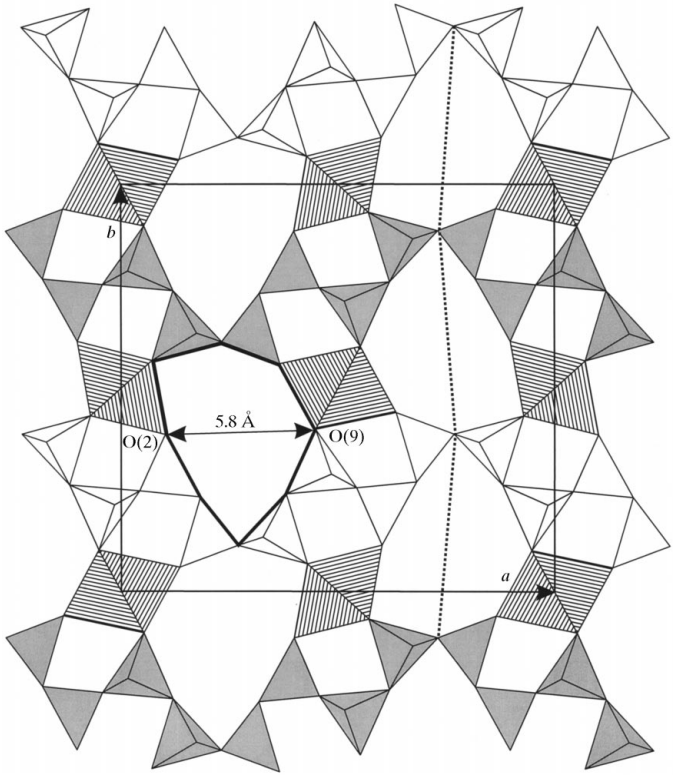

Figure 2
Projection of the structure of α-$K_3NdSi_6O_{15}\cdot 2H_2O$ along [001] showing NdO_6 and SiO_4 polyhedra. The polyhedral edges indicated with bold lines define a channel in the structure that extends along [001]. The dotted line indicates a likely cleavage plane in the structure.

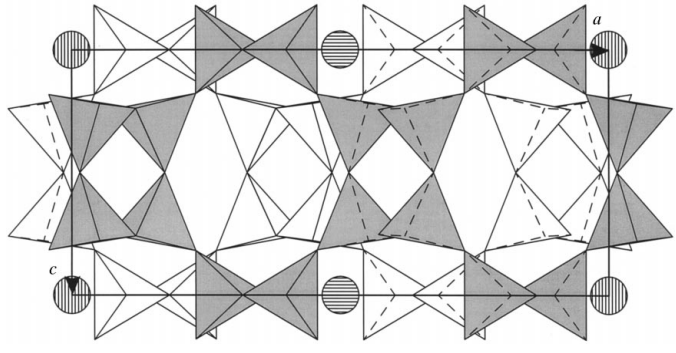

Figure 3
Projection of the structure of α-$K_3NdSi_6O_{15}\cdot 2H_2O$ along [010] showing SiO_4 tetrahedra and Nd atoms. The latter, indicated by hatched circles, occur at $y = 0$ and $\frac{1}{2}$. The shading of the tetrahedra corresponds to that used to distinguish the layer at $y = \frac{3}{4}$, as in Fig. 2.

Table 7
Distances between water molecules and their nearest neighbors.

Ow(1) neighbor	Distance (Å)	Ow(2) neighbor	Distance (Å)	Ow(3) neighbor	Distance (Å)
K(2)^{i}	2.61 (2)	Ow(2)^{ii}	1.15 (4)	Ow(2)	1.67 (3)
O(9), O(9)^{ii}	2.728 (12)	Ow(3)	1.67 (3)	Ow(2)^{ii}	2.51 (3)
Ow(3), Ow(3)^{ii}	3.05 (3)	Ow(3)^{ii}	2.51 (3)	K(1)	2.56 (2)
Ow(2), Ow(2)^{ii}	3.25 (3)	K(3)	2.87 (2)	K(3)	2.73 (2)
O(10)	3.50 (2)	K(2)	2.90 (2)	O(2)	2.80 (2)
		O(8)	3.08 (2)	Ow(3)^{ii}	3.02 (5)
		Ow(1)	3.25 (3)	O(5)^{iii}	3.04 (2)
		K(1)	3.31 (2)	Ow(1)	3.05 (3)
		O(6)	3.37 (2)	O(7)^{iii}	3.18 (2)
		O(3)	3.47 (2)		
		O(1)	3.65 (2)		

Symmetry codes: (i) $-x+\frac{1}{2}, y+\frac{1}{2}, -z+1$; (ii) $x, y, -z+1$; (iii) $-x+\frac{1}{2}, y+\frac{1}{2}, z$.

3.2.2. Interstitial species. Potassium ions and water molecules are located in interstitial sites within the rather open framework of silicate and neodymia polyhedra. The coordination polyhedron about K(2) is rather unusual in that all of its oxygen nearest neighbors lie within the same silicate layer and, accordingly, the 'polyhedron' is almost planar, Fig. 4. The sum of the bond valences about K(2) provided by its six oxygen nearest neighbors and four oxygen second-nearest neighbors is only 0.64, Table 7. While alkali bond-valence sums often deviate from one, particularly for large alkali ions, because of the 'soft' nature of these species, this bond-valence sum would suggest that K(2) is highly underbonded. If, however, one also considers the three oxygen atoms, Ow(1) and Ow(2) (2 ×), coordinating K(2), which belong to interstitial water molecules, the bond-valence sum becomes 0.91, giving further support to our assignment of the residual peaks in the electron-density difference map. Moreover, these water species serve to provide bonds to K(2) both above and below the plane defined by the oxygen ions that are part of a single Si_2O_5 layer and modify the otherwise unusual planar coordination about K(2).

The K(1) and K(3) ions have coordination polyhedra that link neighboring silicate layers, Fig. 5. Both alkali ions reside within large cavities formed by the corrugation in the Si_2O_5 layers. The coordination polyhedron about K(3) is loosely defined by seven nearest-neighbor oxygen atoms and four water molecules. As evident in Fig. 5, five of those oxygen atoms [(O(7) (2 ×), O(10) and O(1) (2 ×)] form part of one silicate layer and two [O(7)′ (2 ×)] belong to a second adjacent layer. The second-nearest neighbors also derive from both silicate layers on either side of K(3). As in the case of K(2), the sum of the bond valences contributed only by non-water oxygen atoms is low, 0.66, however, the interstitial water molecules do not strongly bond to K(3), raising the bond-valence sum to only 0.79. Neighboring K(3) sites are linked by sharing the face formed by the four O(7) atoms.

The K(1) ion resides within the pronounced channel between the Si_2O_5 layers that extends along [001]. It is coor-

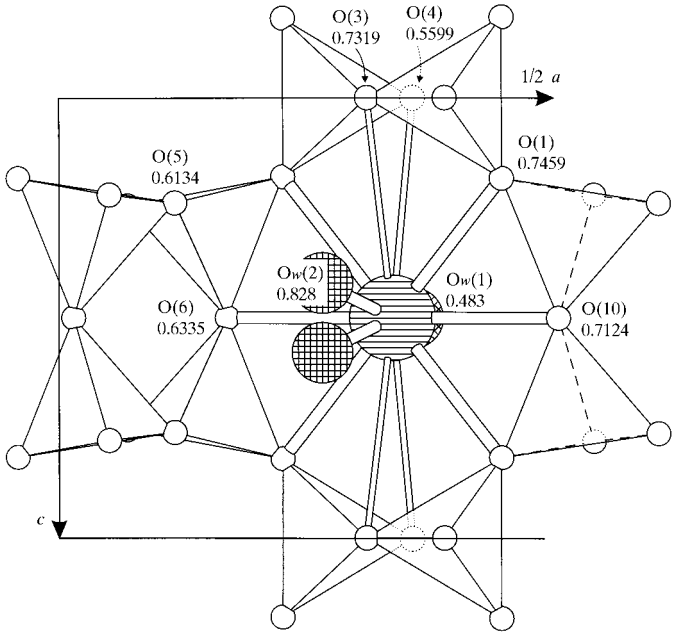

Figure 4
Projection of the structure of α-$K_3NdSi_6O_{15}\cdot 2H_2O$ along [010] from $\sim\frac{1}{2}b$ to $\sim b$ showing the coordination geometry about K(2) located at y = 0.6555. The elevation of O atoms and water molecules is as indicated.

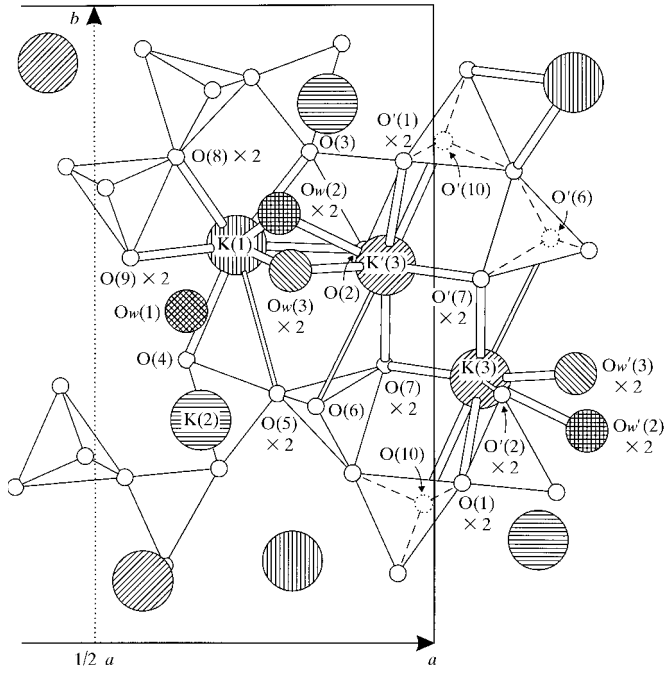

Figure 5
Projection of the structure of α-$K_3NdSi_6O_{15}\cdot 2H_2O$ along [001] showing the coordination geometry about K(1) and K(3). K(1), at elevation 0, is bonded to O(4) at 0, to O(9) at 0.2212 and −0.2212, to O(8) at 0.2396 and −0.2396, to O(3) at 0, to Ow(2) at 0.4207 and −0.4207, to O(2) at 0, and to Ow(3) at 0.2924 and −0.2924. O(5) at 0.1799 and −0.1799 serves as a second-nearest anion neighbor. K(3), at elevation 0.5, is bonded to O(7) and O(7)′ each at elevations 0.25 and 0.75, to Ow(3)′ at 0.2924 and 0.7076, to Ow(2)′ at 0.4207 and 0.5793, to O(1) at 0.1828 and 0.8172, and to O(10) at 0.5. O(6) at 0.5 and O(2)′ at 0 and 1 serve as second-nearest neighbors to K(3). In the vicinity of the K(3) atom, the figure includes all atoms from z = 0 to 1, whereas about K(1), K(2) and K(3)′, atoms at elevations greater than ∼ 0.3 have been omitted for clarity.

dinated by eleven nearest neighbors, seven of which are non-water oxygen atoms. As with the K(3) ion, these oxygen atoms are not evenly distributed between layers on either side of K(2). Six derive from a layer on one side and only one from a layer on the other, although a pair of second nearest neighbors, O(5) (2 ×), also reside within this second layer. The sum of the bond valences about K(1), disregarding the contribution of the water molecules, is 0.72. The water molecules cause this value to rise to 0.96, again, in agreement with the assumption that these interstitial species must indeed be H_2O. The channels within which K(1) is located provide a likely pathway for ion transport. Moreover, the thermal vibration parameter of K(1) along the *c* direction, U^{33}, is quite large, 10.5 (4) × 10^{-2} Å^2, indicating that the potential well is particularly soft along [001] and further supporting the expectation of substantial ionic conduction in this direction.

4. Room-temperature ordering

It was observed that after long annealing periods at room temperature, α-$K_3NdSi_6O_{15}\cdot 2H_2O$ undergoes an ordering transition. Weak superstructure peaks were detected in precession photographs of crystals that had aged for six or more months. In Fig. 6 one such 1*kl* photograph, obtained from a representative crystal seven months after synthesis, is shown. It is evident that the distance between reciprocal lattice points along **b*** and **c*** are approximately equal, and the corresponding real-space parameters turn out to be ∼ 15 Å, which is twice the value of *c* in α-$K_3NdSi_6O_{15}\cdot 2H_2O$. Combining the results of the 1*kl* photo shown in Fig. 6 with 0*kl*, *h*0*l* and *hk*0 photos (not shown) furthermore revealed that the diffraction symbol had changed from *Pbam* to *Pnn**. Accordingly, the space groups *Pnn*2 and *Pnnm* are permitted for the ordered phase. If the latter, centric possibility is selected, the array of ions in a doubled *Pbam* cell (doubled along *c*) can be accommodated in a *Pnnm* structure, in which the new pair of coordinates for each atom are given by (x',y',z') and $(x',y',z'+\frac{1}{2})$ where $x'=x$, $y'=y$ and $z'=\frac{1}{2}z$. The results of this transformation are given in Table 8. All atoms except five retain their site symmetry in the ordered phase. The five exceptions, K(2), K(3) O(6), O(10) and O*w*(1), reside in pairs of 4*h* *x* *y*,$\frac{1}{2}$ special positions of symmetry *m* in space group *Pbam* and move into general positions (of symmetry 1) in the ordered *Pnnm* structure.

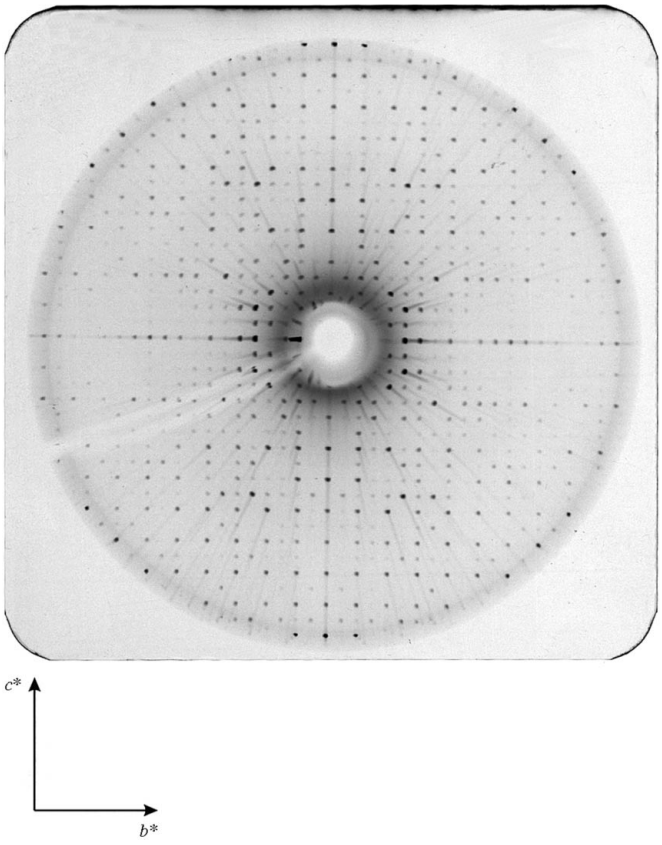

Figure 6
(1*kl*) precession photograph of $K_3NdSi_6O_{15}\cdot 2H_2O$ recorded at room temperature and seven months post-synthesis (α', ordered phase). Photograph recorded with Mo *K*α radiation, 35 kV, 15 mA.

Table 8
A comparison of the (measured) atomic coordinates of α-$K_3NdSi_6O_{15}\cdot 2H_2O$ in the *Pbam* space group with *c* = 7.2794 (7) Å and of the (proposed) *z*-coordinates of the atoms in the ordered phase, α', in space group *Pnnm* with *c* = 14.56 Å.

Atom	*Pbam* position	*Z* = 4 *z*	*Pnnm* position	*Z* = 8 *z*′, *z*′ + 1/2
Nd(1)	2(*a*) ..2/*m*	0	2(*a*) ..2/*m*	0
			2(*b*) ..2/*m*	1/2
Nd(2)	2(*c*) ..2/*m*	0	2(*a*) ..2/*m*	0
			2(*b*) ..2/*m*	1/2
K(1)	4(*g*) ..*m*	0	4(*g*) ..*m*	0
			4(*g*) ..*m*	1/2
K(2)	4(*h*) ..*m*	1/2	8(*h*)	0.2500
K(3)	4(*h*) ..*m*	1/2	8(*h*)	0.2500
Si(1)	4(*g*) ..*m*	0	4(*g*) ..*m*	0
			4(*g*) ..*m*	1/2
Si(2)	8(*i*)	0.2862 (2)	8(*h*)	0.1431
			8(*h*)	0.6431
Si(3)	4(*g*) ..*m*	0	4(*g*) ..*m*	0
			4(*g*) ..*m*	1/2
Si(4)	8(*i*)	0.2821 (3)	8(*h*)	0.1411
			8(*h*)	0.6411
O(1)	8(*i*)	0.1828 (8)	8(*h*)	0.0914
			8(*h*)	0.5914
O(2)	4(*g*) ..*m*	0	4(*g*) ..*m*	0
			4(*g*) ..*m*	1/2
O(3)	4(*g*) ..*m*	0	4(*g*) ..*m*	0
			4(*g*) ..*m*	1/2
O(4)	4(*g*) ..*m*	0	4(*g*) ..*m*	0
			4(*g*) ..*m*	1/2
O(5)	8(*i*)	0.1799 (7)	8(*h*)	0.0900
			8(*h*)	0.5900
O(6)	4(*h*) ..*m*	1/2	8(*h*)	0.2500
O(7)	8(*i*)	0.2459 (8)	8(*h*)	0.1230
			8(*h*)	0.6230
O(8)	8(*i*)	0.2397 (8)	8(*h*)	0.1199
			8(*h*)	0.6199
O(9)	8(*i*)	0.2213 (8)	8(*h*)	0.1107
			8(*h*)	0.6107
O(10)	4(*h*) ..*m*	1/2	8(*h*)	0.2500
O*w*(1)	4(*h*) ..*m*	1/2	8(*h*)	0.2500
O*w*(2)	8(*i*)	0.421 (3)	8(*h*)	0.2105
			8(*h*)	0.7105
O*w*(3)	8(*i*)	0.292 (3)	8(*h*)	0.1460
			8(*h*)	0.6460

Amongst the symmetry elements lost in the *Pbam* to *Pnnm* transformation is a mirror plane at $(x,y,\frac{1}{2})$. Physically, the loss of this symmetry most likely corresponds to the K(2) and K(3) atoms moving slightly away from the centers of their coordination polyhedra. In doing so, these atoms surely lower their rather large thermal parameters. Interestingly, the ordering transition does not move K(1), the atom with the largest thermal displacement parameters, into a site of lower symmetry. In general, the weakness of the superstructure peaks and the relatively unchanged intensity distribution amongst the substructure peaks indicate that the ordering does little to change the overall topology of the structure. Moreover, it should be noted that superstructure peaks were observed in only a few samples. Indeed, the majority of crystals examined even 2–3 years after synthesis did not become ordered.

4.1. High-temperature behavior

4.1.1. Results. The bulk of the high-temperature investigations were carried out on samples which had aged at room temperature for several months, thus the precise state of ordering was not always known. It will be demonstrated, however, that the room-temperature ordering had little effect on the material behavior at high temperatures.

The TGA trace and accompanying mass spectrometry results of an aged sample of α/α'-$K_3NdSi_6O_{15}\cdot 2H_2O$ are presented in Fig. 7. Gradual weight loss began at a temperature of $\sim$ 325 K, reached a maximum at 375 K, and was essentially complete at 525 K, Fig. 7(*a*). This weight loss was mirrored in the mass spectrometry results, which showed a broad water peak centered at $\sim$ 370 K. No other species were detected by mass spectrometry at levels above background.

Representative DSC data obtained from aged α/α'-$K_3NdSi_6O_{15}\cdot 2H_2O$, both on heating and immediately reheating the same sample, are shown in Fig. 8. During the first heating cycle, the compound exhibited two DSC peaks, the first centered at a temperature between 389 and 413 K, depending on the exact sample, and the second between 428 and 433 K. The sum of the heats of these two transitions was 40–50 J g^{-1}. Upon reheating, only one transition could be resolved and this was centered at $\sim$ 473 K, a significantly higher temperature than obtained in the first cycle. Moreover, the heat of transition was lowered to 2.5–5 J g^{-1}. A single DSC measurement of a fresh sample (examined 5 weeks after synthesis) exhibited only one peak in the first heating cycle at 433 K and, somewhat surprisingly, two peaks in the second heating cycle, at 468 and 477 K (not shown). These observations suggest that the number and temperature of the high-temperature transitions are rather independent of the progress of the $\alpha \rightarrow \alpha'$ transformation. However, the heat of transformation from the room-temperature to the high-temperature (> 433 K) phase was correlated to the aging. The value for the fresh sample was only 3.7 J g^{-1}, much lower than obtained for an aged sample in the first heating cycle. In no instance was any DSC trace detected upon cooling, but this is probably because the reverse transition was too sluggish to be detected by thermal methods.

In Fig. 9 the high-temperature X-ray diffraction patterns obtained photographically using the Guinier camera are shown. Crystals of α-$K_3NdSi_6O_{15}\cdot 2H_2O$ used in these experi-

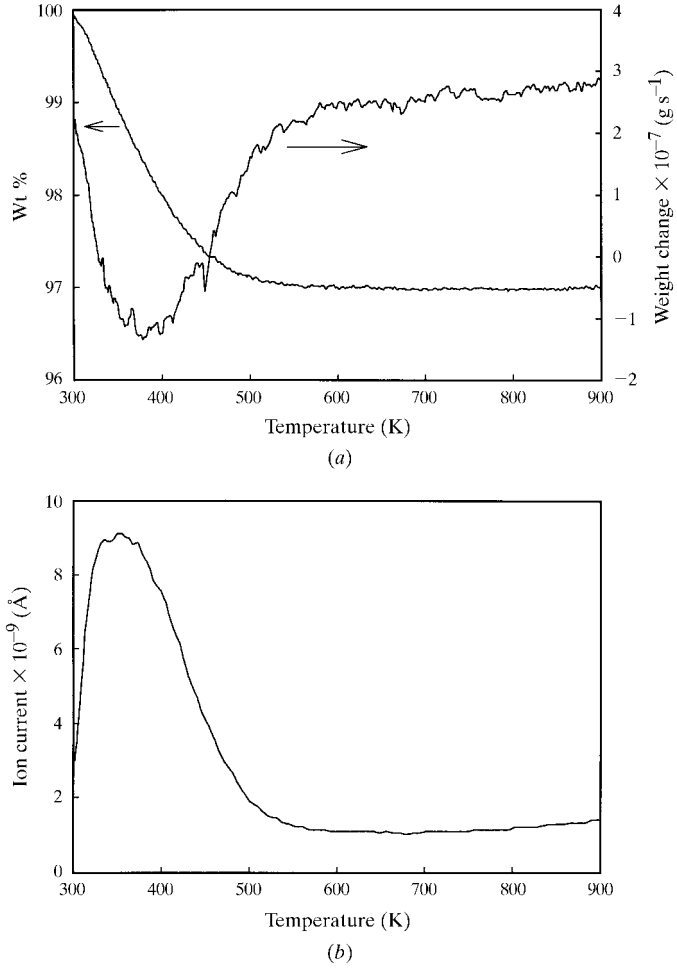

Figure 7
(*a*) Thermogravimetric trace and (*b*) mass spectrometry results of α/α'-$K_3NdSi_6O_{15}\cdot 2H_2O$ obtained upon heating an aged sample.

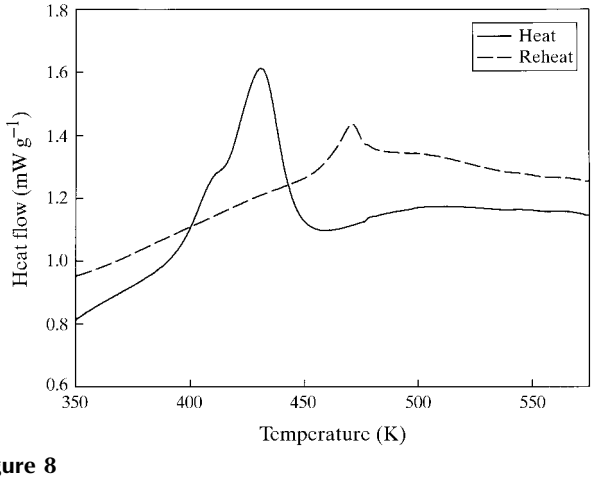

Figure 8
Differential scanning calorimetry trace of α/α'-$K_3NdSi_6O_{15}\cdot 2H_2O$ obtained both upon heating and reheating an aged sample. Data collected in flowing N_2 at 20 K min^{-1} with a Dupont DSC7 instrument.

Table 9
Interplanar spacings of (h00) peaks in $K_3NdSi_6O_{15}\cdot xH_2O$ at various temperatures, and the a lattice constant determined from those spacings.

Peak *hkl*	298 K, pre-heat *d* (Å)	298 K, post-heat *d* (Å)	393 K, on heating *d* (Å)	393 K, on cooling *d* (Å)
200	8.1215	8.0660	7.8588	7.8623
400	4.0361	4.0171	3.9218	3.9252
600	2.6822	2.6743	2.6112	2.6119
a (Å)	16.16 (8)	16.08 (4)	15.69 (3)	15.70 (3)

ments, although aged, were not ordered (*i.e.* did not exhibit superstructure peaks by precession photography). These data, collected during both heating and cooling, clearly demonstrate the existence of two successive phase transitions. The first is to a phase we hereby designate α_I and the second to a phase we designate α_{II}.

In Fig. 10 a 0kl precession photograph of the α_{II} phase recorded at 473 (15) K is shown (we presume that a of the α_{II} phase is parallel to a of the α phase). Owing to the difficulties associated with high-temperature single-crystal diffraction experiments (thermal cracking and degradation of crystal quality), only this photograph was successfully recorded. A close comparison of this zero-level photograph with the corresponding photograph of α-$K_3NdSi_6O_{15}\cdot 2H_2O$ recorded at room temperature, Fig. 15*a* (shown below), reveals that the b^* spacing has halved relative to that of the room-temperature structure. The implication is that either the b lattice parameter has doubled or that the [010] glide in the (100) plane has been removed. The c lattice parameter appears relatively unchanged.

Powder diffraction patterns of $K_3NdSi_6O_{15}\cdot 2H_2O$ obtained at 298, 393 and 493 K are shown in Fig. 11, and are compared with a simulated pattern based on the atomic coordinates given in Table 3. The first room-temperature pattern (collected prior to heating) was virtually identical to that obtained post-heating and, for clarity, is not shown. The enhanced intensity of the (h00) peaks in the room-temperature pattern relative to the simulated pattern reveals that the sample was highly textured along [100]. Given the crystal habit, that of (100) platelets, such texturing is to be expected. Furthermore, at least one impurity phase, $K_8Nd_3Si_{12}O_{32}OH$, was present in the sample examined, as evidenced by the presence of a strong peak at $\sim 7.5^\circ$ 2θ (12 Å). It is apparent from the data in Fig. 11 that, upon heating, strong (h00) peaks shift to larger values of 2θ, implying a reduction in the a lattice constant. The magnitude of a as refined from the powder data and as a function of temperature is provided in Table 9.

4.1.2. Discussion. The high-temperature Guinier photographic data, Fig. 9, clearly demonstrate that the two phase transitions encountered upon heating are reversible in nature. In general agreement with the calorimetry, these X-ray data also revealed the first transition to occur at $\sim$ 391 K and the second at 407 K. The slightly lower transition temperatures measured by the X-ray method as compared to the calorimetric method is probably a consequence of the slower rate, 20 K h^{-1}, used to carry out the former experiment, as compared to the latter, which was carried out at 20 K min^{-1}. It is considered improbable that either of the two transitions observed by X-ray and calorimetric methods are due to reversible dehydration; the loss of water took place gradually and was thus unlikely to produce a thermal effect in the calorimetry experiments. Moreover, the broad peak evident in

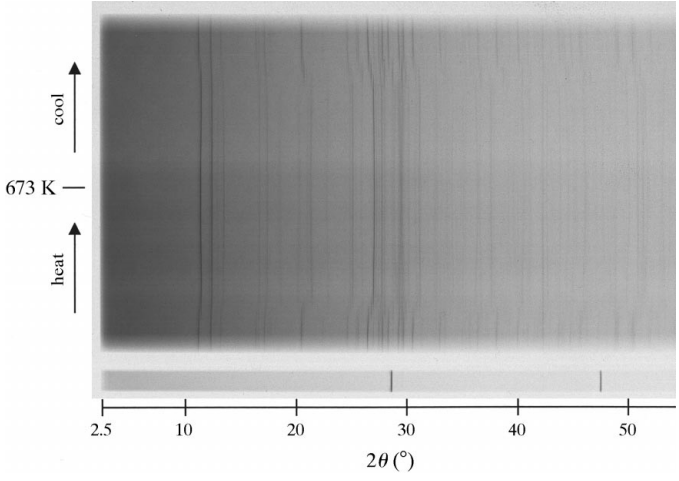

Figure 9
Guinier, X-ray powder diffraction data from α/α'-$K_3NdSi_6O_{15}\cdot 2H_2O$ collected both upon heating and cooling. Notice two reversible phase transitions.

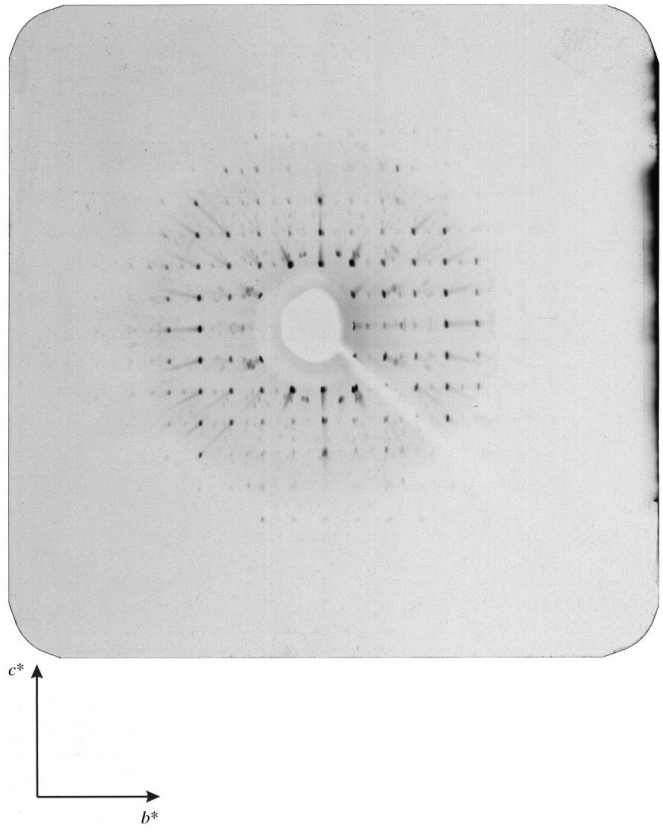

Figure 10
(0kl) precession photographs of α_{II}-$K_3NdSi_6O_{15}$ collected at 473 (15) K.

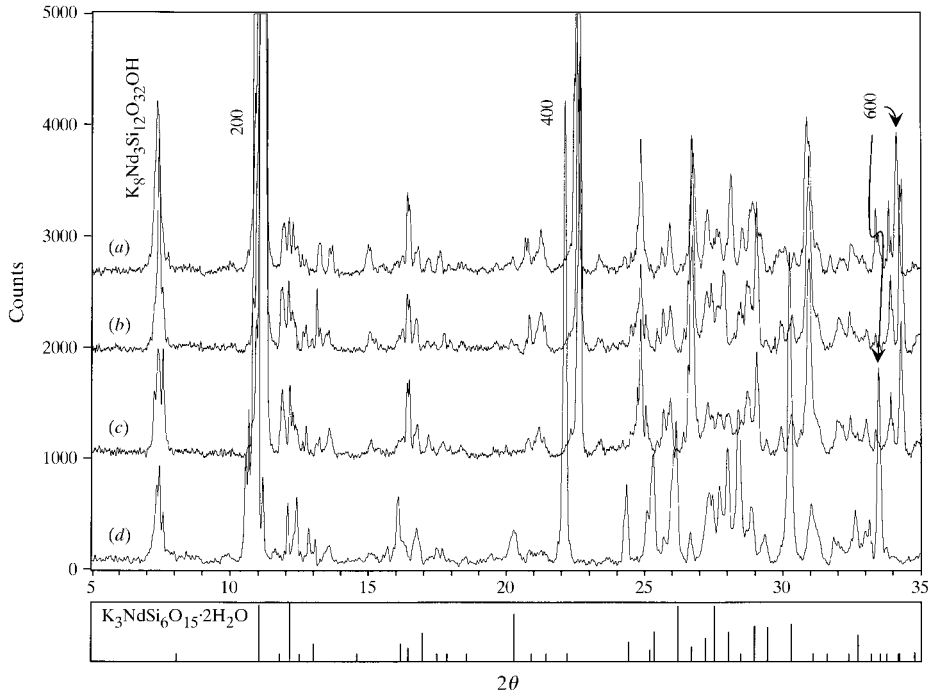

Figure 11
X-ray powder diffractograms of $K_3NdSi_6O_{15}\cdot xH_2O$ upon both heating and cooling: (*a*) 493 K; (*b*) 393 K, upon heating; (*c*) 393 K upon cooling; (*d*) room-temperature, post-heating. Patterns enhanced by background subtraction and smoothing.

the DTGA curve, Fig. 7, occurred at a lower temperature than the sharper phase transitions recorded by DSC, Fig. 8, and high-temperature X-ray diffraction, Fig. 9.

The sequence of transformation can thus be summarized as α (or α') $\overset{400\pm30\ \mathrm{K}}{\longleftrightarrow}$ and α_{I} $\overset{415\pm25\ \mathrm{K}}{\longleftrightarrow}$ α_{II}. Given the temperature range over which dehydration occurred, we conclude that α_{II} is certainly anhydrous and α_{I} may or may not contain residual water. The high-temperature phase, α_{II}, is stable to temperatures of at least 1373 K, as evidenced by the absence of features in the high-temperature DSC data. The lower total enthalpy for the transition from an initially disordered α phase as compared to that from a more ordered phase is consistent with a presumption that α is metastable with respect to the ordered phase α'.

Combining the results of these high-temperature structural studies, we can conclude that the silicate layers likely remain intact at elevated temperatures, as evidenced by the reversibility of the transitions; that the layers are even more corrugated in the high-temperature phases than they are at room temperature, as evidenced by the decrease in the *a* lattice constant; and that the increased corrugation is accompanied by a disruption of the symmetry along **b**, as evidenced by the appearance of additional diffraction spots in the 0*kl* precession photograph of α_{II}-$K_3NdSi_6O_{15}$. The persistence of a corrugated layer structure almost undoubtedly implies the existence of channels between those layers, and these channels, in turn, may be expected to provide pathways for ion transport and lead to high conductivity along [001].

5. Conductivity

The conductivity of single-crystal samples was measured, as stated earlier, at temperatures between 573 and 1193 K, and thus reflect the properties of the α_{II} phase. Lower-temperature measurements could not be made because of the high resistivity of the samples. A typical impedance plot is shown in Fig. 12 in the Nyquist representation of $-Z_{\mathrm{imag}}$ *versus* Z_{real}. As expected for a single-crystal sample, a single

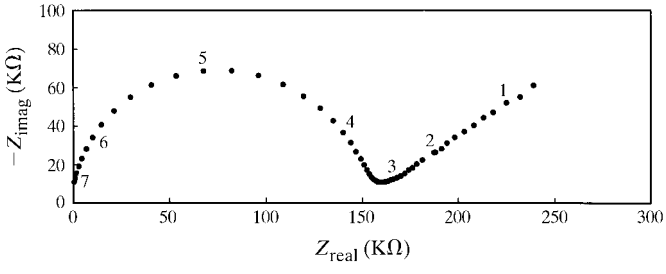

Figure 12
Electrical impedance of α_{II}-$K_3NdSi_6O_{15}$ as a function of frequency presented in a Nyquist plot, Z_{imag} *versus* Z_{real}. Data collected at 1128 K along the *a* axis.

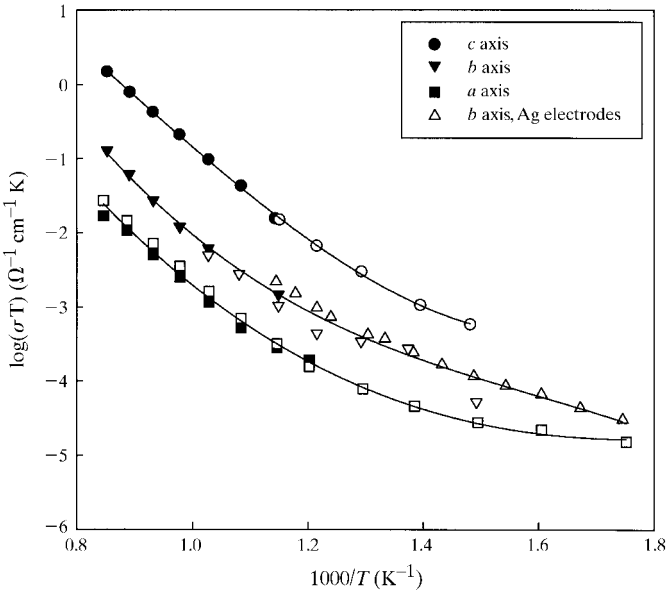

Figure 13
Conductivity of α_{II}-$K_3NdSi_6O_{15}$ as a function of temperature and crystallographic direction. Unless otherwise stated, platinum served as the electrode material. Data points shown with an open symbol were obtained using the Wayne–Kerr instrument, and those with a closed symbol using the HP instrument. Solid lines are guides to the eye. In the case of σ_{11}, data from two different samples have been averaged.

Table 10
Electrical properties of α_{II}-$K_3NdSi_6O_{15}$.

σ_{11}	ΔE_a (eV) High temperature	ΔE_a (eV) Low temperature	σ(873 K) $\times 10^5$ (Ω cm^{-1})
σ_{11}	1.1	0.3	3.4
σ_{22}, Ag	–	0.6	5.8
σ_{22}	1.3	0.7	6.9
σ_{33}	1.3	0.8	17

arc is evident in the data (Macdonald, 1988). The bulk resistance was taken from the intercept of this arc with the real axis. The data point collected at a frequency of 10^4 Hz lies on the arc, ensuring that the data collected with the single-frequency Wayne–Kerr bridge reflect the bulk properties of α_{II}-$K_3NdSi_6O_{15}$. Owing to the wide electronic band-gap typical of alkali silicates, the measured conductivity is assumed to be entirely ionic.

The conductivity as a function of temperature for each crystallographic direction is shown in Arrhenius form, $\log(\sigma T)$ *versus* $1/T$, in Fig. 13. It is apparent that the electrical behavior is not strictly Arrhenius; the conductivity along each direction increases with temperature at a faster rate than would be expected for a simple activated process. It is unlikely that this upward curvature is the result of a phase transition as none was detected by thermal analysis in the temperature region over which conductivity data were collected. From the slopes of these curves in high- and low-temperature regions of Fig. 13, we obtain the values for the activation energy given in Table 10. For comparative purposes, the conductivity at 873 K is also listed in the table.

The results shown in Fig. 13 reveal that σ_{33} is the largest term in σ_{ij}, indicating that the [001] channels do indeed provide a convenient pathway for ion transport. The greater magnitude of σ_{22} over σ_{11} furthermore suggests that motion through the layers (*via* whatever rings may exist within them after transformation to the α_{II} phase) is easier than motion perpendicular to the corrugation. While the relative magnitudes of the conductivities along the three axes correspond well to structural features, the activation energies follow the

Figure 14
Optical photograph of α/α'-$K_3NdSi_6O_{15}$·$2H_2O$ before and after Ag^+ ion exchange.

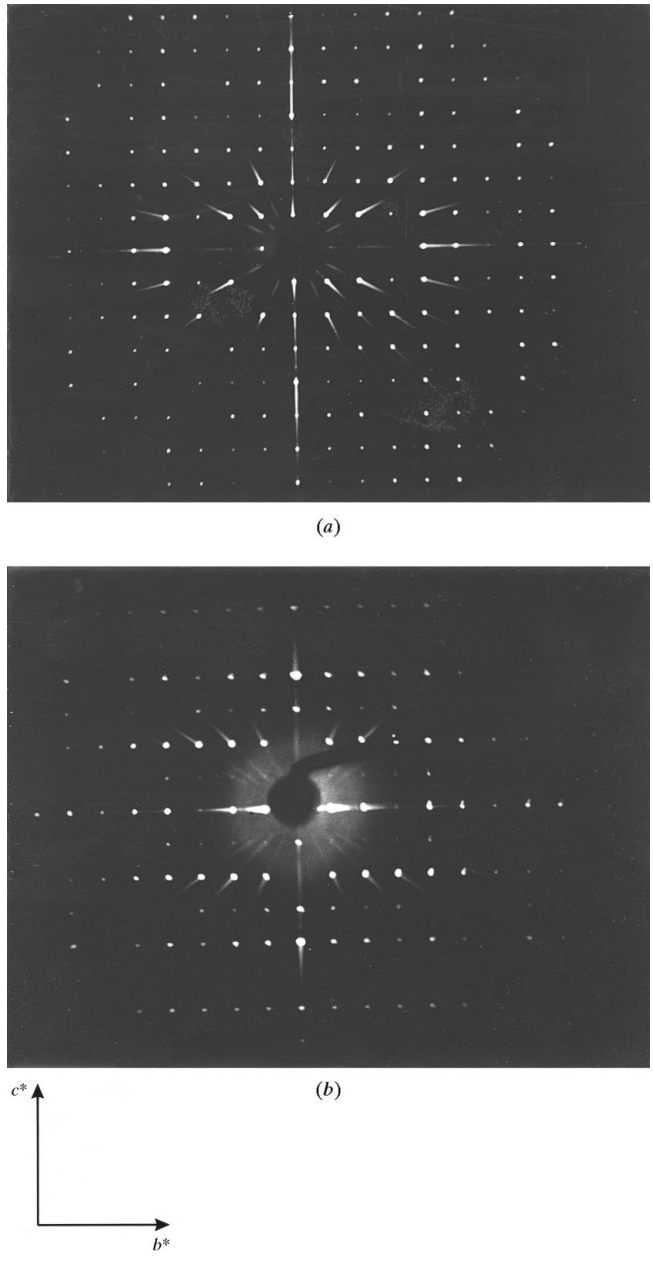

Figure 15
(0*kl*) precession photographs of α-$K_3NdSi_6O_{15}$·$2H_2O$ (*a*) prior to and (*b*) after Ag^+ ion exchange. Photographs recorded at room temperature with Mo $K\alpha$ radiation, 35 kV, 15 mA.

opposite trend. This, combined with the temperature dependence of ΔE_a, suggests that a simple, isolated ion-hopping model, which would lead to Arrhenius behavior, is inadequate for describing the conduction process in α_{II}-$K_3NdSi_6O_{15}$.

6. Ion exchange

Silver ion exchange experiments resulted in a definite change in the color of crystals from transparent or opaque/white to a dark amber-brown, as can be seen in Fig. 14, an optical photograph of both as-synthesized and ion-exchanged samples. Crystals shown in the photograph were cleaned utrasonically before examination to ensure that the discoloration was not simply due to surface precipitation of some other phase. A similar change in color was observed in crystals used for electrical characterization when Ag was utilized as the electrode material. Despite the ease with which it occurred, the exchange of K^+ for Ag^+ in α/α'-$K_3NdSi_6O_{15}\cdot 2H_2O$ caused a great deal of structural change. In Fig. 15 the $0kl$ photographs of a crystal prior to and after ion-exchange are compared. The $l = 2n + 1$ spots of the ion-exchanged sample are greatly diminished in intensity, indicative of strong pseudosymmetry along **c**.

These preliminary optical and structural results suggest that K^+ can readily be replaced with Ag^+. Complete compositional, structural and electrical characterization of the ion-exchanged material is underway and will be the subject of a future report. It should be noted, however, that (as can be seen in Fig. 13) the conductivity of α_{II}-$K_3NdSi_6O_{15}\cdot 2H_2O$ measured with silver electrodes was no greater than that measured with platinum electrodes. Furthermore, the conductivity was not a function of time, despite the incorporation of Ag from the electrodes, as had been the case with $K_3NdSi_6O_{15}\cdot 2H_2O$ [Hale (*sic*) *et al.*, 1993]. These observations suggest that although Ag can be quite easily incorporated into α/α'-$K_3NdSi_6O_{15}\cdot 2H_2O$, ion exchange may not be a fruitful route towards an even higher conductivity material.

The authors gratefully acknowledge the contributions of several colleagues to this work. Dr Karl Peters of the Max Planck Institut (MPI) für Festkörperforschung kindly measured single-crystal intensity data, Herr Florian Viczian (MPI) performed high-temperature powder diffractometer experiments, Herr Willie Rötenbach (MPI) collected high-temperature Guinier film data and Frau Nubia Carioca (MPI) conducted the thermal analysis and mass spectroscopy. Mike Jercinovic of the Massachusetts Institute of Technology (MIT) carried out microprobe analyses. The authors also thank Professor Harry Tuller (MIT) for providing access to his electrical characterization laboratory. SMH thanks Dr Joachim Maier for hosting her visit to the Max Planck Institut für Festkörperforschung, where some portions of this research were carried out. This work is dedicated to the memory of the late Robert A. Laudise, a brilliant scientist and exemplary human being who provided invaluable guidance in the method of hydrothermal synthesis. His friendship and inspiration are deeply missed by those who were fortunate to know him.

References

Brown, I. D. & Altermatt, D. (1985). *Acta Cryst.* B**41**, 244–247.
Buerger, M. J. & Prewitt, C. T. (1961). *Proc. Natl. Acad. Sci.* **47**, 1884–1888.
Cromer, D. T. & Waber, J. T. (1974). *International Tables for X-ray Crystallography*, Vol. IV, Table 2.2A, pp. 128–134. Birmingham: Kynoch Press. (Present distributor Kluwer Academic Publishers, Dordrecht.)
Fleet, S. G. (1965). *Z. Kristallogr.* **121**, 349–368.
Haile, S. M., Siegrist, T., Laudize, R. A. & Wuensch, B. J. (1991). *Mater. Res. Soc. Symp. Proc.* **210**, 645–650.
Haile, S. M. & Wuensch, B. J. (1997). *Am. Mineral.* **82**, 1141–1149.
Haile, S. M. & Wuensch, B. J. (2000). *Acta Cryst.* B**56**, 349–362.
Haile, S. M., Wuensch, B. J., Laudise, R. A. & Maier, J. (1997). *Acta Cryst.* B**53**, 7–17.
Haile, S. M., Wuensch, B. J., Laudise, R. A., Opila, R., Siegrist, T. & Foxman, B. (1991). *Trans. Am. Cryst. Assoc.* **27**, 77–94.
Haile, S. M., Wuensch, B. J., Siegrist, T. & Laudise, R. A. (1993). *J. Cryst. Growth*, **131**, 352–372.
Hale (*sic*), Maier, J., Wuensch, B. J. & Laudise, R. A. (1993). *Proc. NATO Workshop Fast Ion Transport in Solids*, edited by B. Scrosati, pp. 315–326. Amsterdam: Kluwer Academic Publishers.
Kudoh, Y. & Takeuchi, Y. (1979). *Mineral. J. Jpn*, **9**, 349–373.
Laudise, R. A. (1987). *Advanced Crystal Growth*, edited by P. M. Dryburgh, B. Cockayne and K. G. Barraclough. New York: Prentice Hall.
Liebau, F. (1962). *Naturwiss.* **49**, 481–491.
Liebau, F. (1987). *Structural Chemistry of Silicates: Structure, Bonding, and Classification.* Berlin: Springer-Verlag.
MacDonald, J. R. (1988). *Impedance Spectroscopy*. New York: Wiley and Sons.
Pushcharovskii, D. Yu., Karpov, O. G., Pobedimskaya, E. A. & Belov, N. V. (1977). *Sov. Phys. Dokl.* **22**, 292–293.
Schamber, F., Wodke, N. & McCarthy, J. (1981). *ZAF Matrix Correction Procedure for Bulk Samples: Operation and Program Description*, 31 pp. Tracor Northern, Publication TN-2120, Middleton, Wisconsin, USA.
Shannon, R. D. & Prewitt, C. T. (1969). *Acta Cryst.* B**25**, 925–946.
Sheldrick, G. M. (1993). *Crystallographic Computing*6, edited by H. D. Flack, L. Parkanyi and K. Simon, pp. 100–110. New York: Oxford University Press.
Simon, V. A. (1971). *J. Appl. Cryst.* **4**, 138–145.
Taylor, W. H. & Náray-Szabó, S. (1931). *Z. Kristallogr.* **77**, 146–158.